NANO LETTERS

Letter

pubs.acs.org/NanoLett

Composition-Graded Nanowire Solar Cells Fabricated in a Single Process for Spectrum-Splitting Photovoltaic Systems

Derek Caselli, Zhicheng Liu, David Shelhammer, and Cun-Zheng Ning*

ASU Nanophotonics Lab, Arizona State University, Tempe, Arizona 85287, United States

Supporting Information

ABSTRACT: Nanomaterials such as semiconductor nanowires have unique features that could enable novel optoelectronic applications such as novel solar cells. This paper aims to demonstrate one such recently proposed concept: Monolithically Integrated Laterally Arrayed Multiple Band gap (MILAMB) solar cells for spectrum-splitting photovoltaic systems. Two cells with different band gaps were fabricated simultaneously in the same process on a single substrate using spatially composition-graded CdSSe alloy nanowires grown by the Dual-Gradient Method in a chemical vapor deposition system. CdSSe nanowire ensemble devices tested under 1 sun AM1.5G illumination achieved open-circuit voltages up to 307 and 173 mV and short-circuit current densities as high as 0.091 and 0.974 mA/cm^2 for the CdS- and CdSe-rich cells, respectively. The open-circuit voltages were roughly three times those of similar CdSSe film cells fabricated for comparison due to the superior optical quality of the nanowires. $I-V$ measurements were also performed using optical filters to simulate spectrum-splitting. The open-circuit voltages and fill factors of the CdS-rich subcells were uniformly larger than the corresponding CdSe-rich cells for similar photon flux, as expected. This suggests that if all wires can be contacted, the wide-gap cell is expected to have greater output power than the narrow-gap cell, which is the key to achieving high efficiencies with spectrum-splitting. This paper thus provides the first proof-of-concept demonstration of simultaneous fabrication of MILAMB solar cells. This approach to solar cell fabrication using single-crystal nanowires for spectrum-splitting photovoltaics could provide a future low-cost high-efficiency alternative to the conventional high-cost high-efficiency tandem cells.

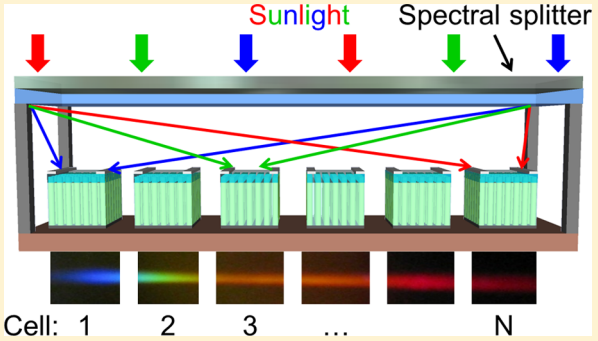

KEYWORDS: *Nanowires, solar cells, spectrum-splitting, composition-graded, semiconductor alloys*

The development of photovoltaic (PV) technology has long been hampered by the choice between low efficiency cells at low cost and high efficiency with prohibitively high cost for terrestrial applications. A paradigm shift in solar cell design and concepts with newly available materials and fabrication technology is needed to break this fundamental dilemma in order to develop solar cells with high efficiency at low cost. The traditional approach to high efficiency PVs is the multijunction tandem cell. The required equipment, the substrate, and the growth and fabrication techniques all make such tandem cells too expensive for wide adoption. In addition, the stringent lattice matching requirement makes further addition or optimization of junctions very challenging.

Spectrum-splitting PV has been pursued as an alternative to the vertical tandem structure for a long time, beginning with the first experimental demonstration in 1978.[1] Impressive results have been achieved over the last several decades,[2−14] especially recently.[10−14] The essence of such lateral or horizontal designs is the use of spectral splitting optics before absorption of sunlight by the cells and the absence of tunnel junctions. However, traditional approaches to spectrum-splitting PV have required fabricating each of the various cells separately with different processes, often on different substrates. As the number of subcells increases, this quickly causes the manufacturing process to become complex and expensive.

Nanomaterials such as nanowires have attracted great attention as important solar cell materials[15−24] and can offer unique advantages for addressing this problem, potentially providing the new paradigm to break the deadlock between efficiency and cost. One of the greatest advantages of nanowires is the ability to grow materials epitaxially from a given substrate with larger tolerance to lattice mismatch than planar structures or nonepitaxially from any substrate with high crystal quality. These advantages enable growth of very dissimilar materials on a single substrate with a wide range of band gaps required for spectrum-splitting PV systems. To utilize such growth advantages to the largest extent possible, we have recently developed a Dual-Gradient Method[25] to grade the alloy composition over a wide range on a given substrate in a single, inexpensive chemical vapor deposition (CVD) run. This is accomplished by carefully engineering gradients in both the temperature[26] across the surface of the substrate and the

Received: July 14, 2014
Revised: August 15, 2014
Published: September 9, 2014

 © 2014 American Chemical Society dx.doi.org/10.1021/nl502662h | *Nano Lett.* 2014, 14, 5772−5779

composition of the source vapor impinging on it to establish local conditions conducive to the growth of different alloy compositions at different locations along the substrate surface.[25] Alloys with band edge emission over the entire visible spectrum were demonstrated with sufficiently high crystal quality to achieve widely tunable lasing.[26] Materials grown in this way could provide inexpensive full-spectrum absorbers for multiple cells in spectrum-splitting PV systems on the same substrate in a single growth process run. Using this unique materials capability, we have recently proposed that it may be possible to simplify the manufacturing and cut costs by integrating the various cell fabrication processes[27,28] to create Monolithically Integrated Laterally Arrayed Multiple Band gap (MILAMB) cells (illustrated in Figure 1). Such a system could

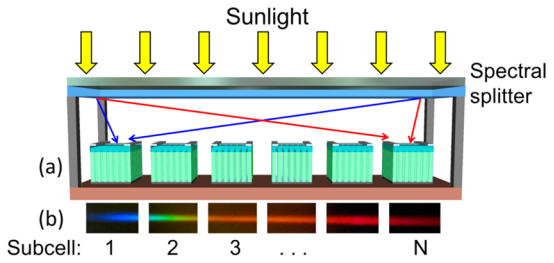

Figure 1. Conceptual diagram of a MILAMB solar cell module (a) where the NW cells are fabricated on a single substrate and integrated with spectrum-splitting optics. Real color photoluminescence from ZnCdSSe NWs[25] (b) grown by the Dual-Gradient Method on a single substrate illustrates the ability to vary the cell band gaps across a wide range in a single growth step.

in principle achieve similar efficiencies to other spectrum-splitting PV systems, which have already demonstrated high efficiencies in the 30 and 40% range[10−14] and are targeting 50%[8,9] but at significantly reduced cost. The MILAMB cells and associated fabrication would use only thin-film-type equipment; no high quality single crystal substrates are required. Such advantages coupled with the simple, one-step NW growth and simultaneous fabrication of subcells could potentially provide an alternative path to achieving high efficiencies competitive with tandem solar cells, yet at a low cost similar to thin film cells in the long run.

In this work, we report the first proof-of-concept demonstration of a MILAMB structure with two subcells fabricated simultaneously in the same process on a single substrate using spatially composition-graded CdSSe alloy NWs. The basic structure of these devices is illustrated in Figure 2. Open-circuit voltages (V_{oc}) of up to 307 and 173 mV were demonstrated for the CdS-rich and CdSe-rich cells, respectively, and were substantially higher, roughly by a factor of 3, than similar composition-graded CdSSe thin film cells

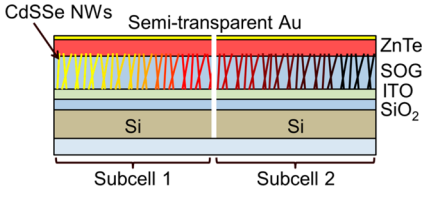

Figure 2. Diagram of the proof-of-concept composition-graded CdSSe NW ensemble solar cells fabricated simultaneously on a single substrate in this study.

fabricated for comparison. Short-circuit current densities (J_{sc}) were on par with those of comparable film cells for some CdSe-rich subcells but were typically in the range of ∼3−15 times lower for the CdS-rich subcells due to spin-on glass (SOG) burying some of the wires. *I*−*V* measurements were also taken using optical filters to simulate spectrum-splitting and compare the CdS- and CdSe-rich subcells for similar above-band gap photon flux. Although the cells were not current-matched at this stage, the V_{oc}'s and FFs of the CdS-rich cells were uniformly larger than the corresponding CdSe-rich cells. This suggests that the wide-band gap CdS-rich cell had greater output power density than the CdSe-rich cell on the single-NW level under their respective designed spectra, as expected, which is the key benefit of spectrum-splitting that enables high efficiencies. These results constitute a proof-of-principle demonstration of the MILAMB approach to fabricating multiple cells for spectrum-splitting PV systems. This approach could potentially provide a low cost alternative to multijunction tandems for achieving high efficiencies.

Results and Discussion. *CdSSe Absorber.* Our earlier design and simulation study[27] predicted that a system of six cells based on CdPbS alloy NWs could achieve efficiencies in the 30−40% range, depending upon the level of solar concentration, in a similar range as many experimental demonstrations of spectrum-splitting PV in literature.[10−14] There are also other material systems that could be more appealing in the long run, such as InGaN,[29] as it also provides full spectral coverage and the material system is better developed. However, CdSSe was selected for the present work because we have already demonstrated spatially composition-graded CdSSe NW ensembles with band gaps spanning the entire composition range.[25,26] Although this system does not contain sufficiently small band gaps to make a high efficiency solar cell, it is adequate for a proof-of-concept study with two subcells.

In addition to the composition-graded CdSSe NW ensemble cells, similar thin film cells were also fabricated for comparison. Growth of composition-graded thin films was also accomplished by the Dual-Gradient Method in similar fashion to the NW cells. The optical quality and band gaps of the spatially composition-graded CdSSe materials grown by the Dual-Gradient Method as functions of position were characterized by microphotoluminescence (PL) scans at intervals along the lengths of the samples, as described in more detail in the Experimental Section. The optical quality of the CdSSe NWs grown in this study was found to be superior to the films, which had PL spectra dominated by defect emission. PL spectra taken at various positions along the substrate lengths are shown in Figure 3 for a CdSSe NW ensemble (a) and film (b). As seen from the PL spectra of the two samples, the intensity ratio of the band edge emission of the NWs to that of the defect (midgap) emission is roughly 3 to 1, while this ratio for thin films is 1 to 7. This indicates roughly a factor of 20 improvement of the band edge emission of NWs over thin films. Relative emission intensities of band edge versus midgap emission are an important measure of the optical quality of the grown semiconductors. The higher optical quality of NWs than thin films illustrates the advantages of using VLS-grown NWs for such cells. Figure 4 shows the optical band gap extracted from PL scan as a function of position for two spatially composition-graded CdSSe NW and film samples. Continuous band gap variation from 2.36 to 1.79 and 2.21 to 1.79 eV was achieved along the substrate length for the NW and film

dx.doi.org/10.1021/nl502662h | *Nano Lett.* 2014, 14, 5772−5779

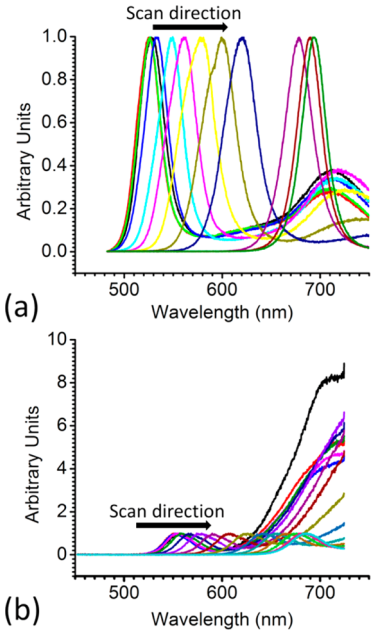

Figure 3. Collected photoluminescence spectra from a spatially composition graded CdSSe (a) NW ensemble and (b) film, scanned from left to right along the lengths of the samples. Defect emission around 750 nm is relatively small compared to band edge emission for the NW ensemble (a) but dominant in the case of the film (b).

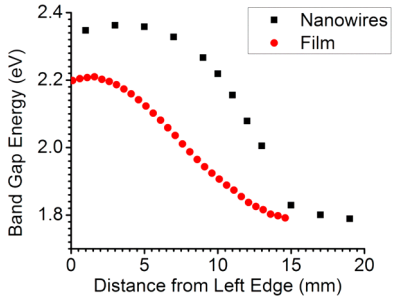

Figure 4. Band gaps of a spatially composition-graded CdSSe NW ensemble and film versus position, as measured by photoluminescence scan.

samples, respectively. This information was used to determine where to divide the samples into two subcells. In order to provide similar levels of above-band gap photon flux to both subcells under spectrally filtered illumination, the samples were cleaved at a location corresponding to a wavelength of approximately 620 nm.

The better optical quality of the NWs and higher V_{oc}'s of the resulting cells (discussed below) suggest that in the long term the superior, single-crystal quality achievable with NWs could allow for higher efficiencies. Their small cross sections could also enable the synthesis of full-spectrum metastable alloys, such as InGaN[29] and CdPbSSe[30] with compositions spanning their full ranges, which would not be possible with film materials. Furthermore, the NW-based approach would in principle use less material and can achieve comparable or more absorption owing to light trapping effects in NW arrays. This makes the NWs more attractive in the long term.

Cell Performance Results. *I*–*V* curves of composition-graded CdSSe NW ensemble cells and similar thin film cells fabricated for comparison under 1 sun AM1.5G illumination are shown in Figures 5 and 6, respectively, and their performance is summarized in Table 1. Note that the transmission of the

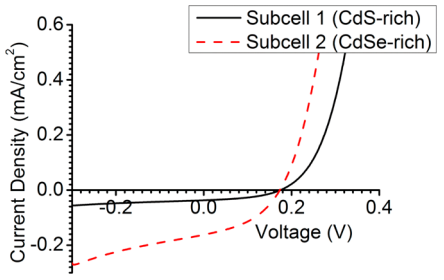

Figure 5. *I*–*V* characteristics of two spatially composition-graded CdSSe NW ensemble solar cells (sample 0219B) fabricated in the same process on a single substrate under identical 1 sun AM1.5G illumination.

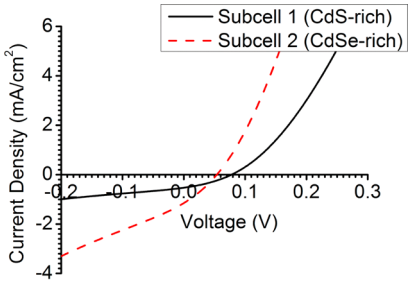

Figure 6. *I*–*V* characteristics of two cells fabricated in the same process on one substrate from a spatially composition-graded CdSSe film (sample 0827O) under identical 1 sun AM1.5G illumination.

semitransparent Au top contact was roughly 40% for wavelengths of interest, so the effective illumination intensity was reduced accordingly (see Supporting Information for more detail). The NW ensemble cells achieved values of V_{oc} as high as 307 mV for the CdS-rich cells and 173 mV for the CdSe-rich cells, while the V_{oc}'s of comparable thin film cells were less than 100 mV for both subcells. Figure 7 shows a graphical comparison of the V_{oc} and J_{sc} of the CdSSe NW and thin film cells for both subcells. The V_{oc}'s of typical NW cells were found to be significantly higher, roughly by a factor of 3. Their fill factors (FF) were also higher, exceeding 40% for both the CdS- and CdSe-rich subcells, whereas the film cells showed FFs of around 33% or less. This is attributed to higher crystal quality in the NWs as compared to the films, as indicated by their stronger band edge emission relative to midgap emission (Figure 3). Note that while literature on similar NW cells using these materials is relatively scarce, a recently reported CdSe/ZnTe core–shell single-NW solar cell achieved V_{oc} and FF of 180 mV and 38%, respectively, similar to the results obtained in this work.[31]

Values of J_{sc} for the NW ensemble cells were promising for unaligned wires when compared with the film cells and were on par with them in the case of some CdSe-rich subcells, as shown in Figure 7. However, typical values were somewhat lower for the NW cells, especially in the case of the CdS-rich subcells, where the J_{sc} was ~3–15 times lower than the film cells. This is attributed to the relatively thick methylsilsesquioxane (MSQ) layer (approximately 4 μm, as shown in Figure 8) and unoriented nature of the NW array, which causes some NWs to be buried by the SOG, preventing them from being contacted and contributing to the output of the device. It is believed that

dx.doi.org/10.1021/nl502662h | *Nano Lett.* 2014, 14, 5772–5779

Table 1. Performance Data for CdSSe NW and Thin Film Solar Cells with 40% Transparent Au Top Contacts under 1 sun AM1.5G Illumination with Values Measured under Spectrally Filtered Illumination Shown in Parentheses

sample ID	cell type	V_{oc} (mV)	J_{sc} (mA/cm^2)	FF
0522N	CdS-rich NWs (thick SU-8)	307 (279)	1.03×10^{-3} (5.48×10^{-4})	30.7% (31.1%)
	CdSe-rich NWs (thick SU-8)	133 (74)	1.43×10^{-4} (2.74×10^{-5})	34.3% (30.1%)
0219B	CdS-rich NWs	175 (151)	0.037 (0.019)	42.9% (41.1%)
	CdSe-rich NWs	173 (132)	0.162 (0.050)	41.2% (37.7%)
0219C	CdS-rich NWs	172 (145)	0.091 (0.039)	40.7% (38.7%)
	CdSe-rich NWs	136 (70)	0.349 (0.109)	32.3% (26.7%)
1122AG	CdS-rich NWs	142 (119)	0.046 (0.024)	37.7% (35.9%)
	CdSe-rich NWs	83 (24)	0.089 (0.015)	29.7% (25.7%)
0219D	CdS-rich NWs	85 (56)	0.045 (0.020)	30.6% (27.9%)
	CdSe-rich NWs	92 (46)	0.974 (0.337)	29.7% (26.4%)
0827O	CdS-rich film	78 (55)	0.530 (0.268)	33.2% (31.0%)
	CdSe-rich film	54 (15)	1.152 (0.226)	29.3% (25.8%)
0827X	CdS-rich film	14 (8)	0.286 (0.144)	25.2% (24.9%)
	CdSe-rich film	23 (6)	0.354 (0.081)	25.1% (24.5%)

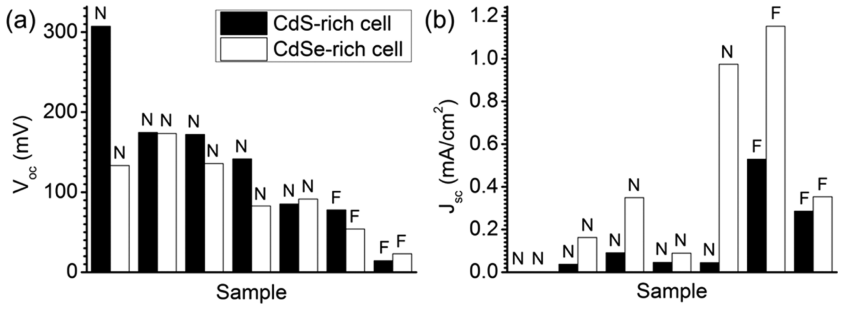

Figure 7. Comparison of the V_{oc} (a) and J_{sc} (b) of CdS- and CdSe-rich NW and thin film solar cells under unfiltered AM1.5G illumination. NW and thin film cells are designated N and F, respectively.

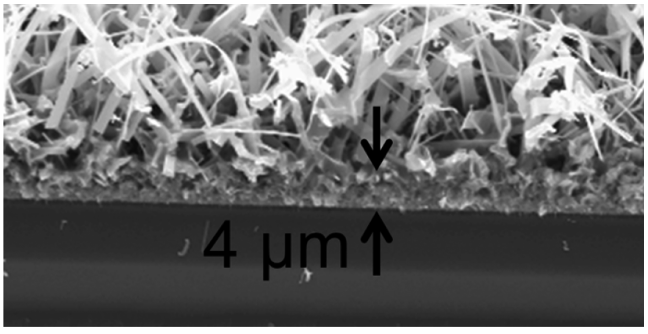

Figure 8. Cross-sectional SEM image of a CdSSe NW ensemble after MSQ application. The MSQ layer is found to be approximately 4 μm thick.

some of the wires growing at shallower angles from the substrate were completely covered by the MSQ, particularly in the case of the CdS-rich compositions, where the morphology tended to favor smaller, denser wires rather than larger, sparser, and more tapered belts, as in the case of Se-rich wires. This also explains why the CdS-rich cells tended to show much smaller J_{sc}'s yet higher V_{oc}'s than the corresponding CdSe-rich cells. If the J_{sc}'s of the CdS-rich cells were genuinely much smaller than those of the CdSe-rich cells on a single-NW level, one would expect their V_{oc}'s to be smaller as well, but this is not observed. For those CdSe-rich NW cells using MSQ wherein the J_{sc} was on par with the film cells, it is believed that the NWs were sufficiently large relative to the MSQ layer thickness that the number of NWs buried by the dielectric material was negligible.

An extreme example of this phenomenon is sample 0522N, which used a thicker spin-on dielectric (SU-8) in place of the MSQ used by all other NW cells. The SU-8 layer was approximately 12 μm thick and despite demonstrating relatively high V_{oc}, the J_{sc} of these cells was roughly two to three orders of magnitude lower than those fabricated using MSQ. The high V_{oc} suggests a reasonably high local J_{sc} within individual wires. Thus, the low measured value of J_{sc}, which is calculated with respect to the macroscopic illuminated area of the device, indicates that the insulating SU-8 layer buries many of the NWs and renders much of the cell area inactive. This was confirmed by scanning electron microscopy (SEM), as shown in Figure 9. Similarly, it is believed that the lower J_{sc} in the NW ensemble cells fabricated with MSQ than the film cells is explained by some of the wires being buried by insulating MSQ, albeit a far greater number of wires are contacted when using MSQ versus SU-8.

While the measured J_{sc} is thus largely an extensive property indicative of the number of NWs that are contacted by the ZnTe layer, the V_{oc} and FF are intensive properties indicative of the photovoltaic performance of those NWs that actively participate in the operation of the device. In this respect, the results in Table 1 and Figure 7 show that the NW ensemble cells clearly outperform similar film cells. This suggests that if all NWs can be contacted, the efficiency of the NW ensemble cells should exceed that of comparable film devices. This could be achieved by adopting a scheme for growing more vertically aligned wires (e.g., using growth templates), substituting a thinner formulation of SOG, or etching to thin the SOG and uncover additional wires.

dx.doi.org/10.1021/nl502662h | Nano Lett. 2014, 14, 5772−5779

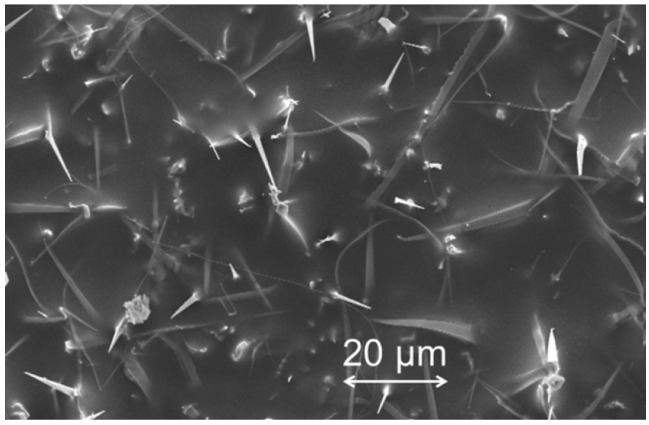

Figure 9. SEM image of a CdSe NW ensemble after spin-coating with thicker SU-8 rather than MSQ, where the SU-8 appears to cover many of the NWs.

I–*V* measurements were also taken under filtered illumination (values reported in Table 1 in parentheses) to simulate a simple form of spectrum-splitting and provide a comparison between the CdS- and CdSe-rich subcells under similar above-band gap photon flux. The *I*–*V* characteristics of a NW ensemble solar cell under filtered illumination are shown in Figure 10 for both the CdS- and CdSe-rich subcells.

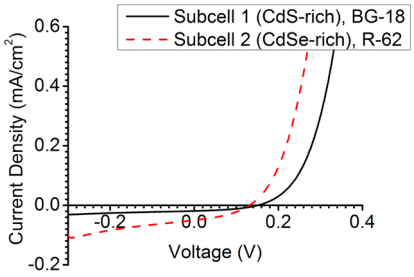

Figure 10. *I*–*V* characteristics of two spatially composition-graded CdSSe NW ensemble solar cells (sample 0219B) fabricated in the same process on a single substrate under spectrally filtered illumination.

In the NW ensemble cells fabricated in this work, the illuminated area was the same for both subcells, but J_{sc} was dependent on the number of NWs contacted, which may vary depending on the morphology and therefore composition of the wires. The results suggest that generally fewer NWs were contacted in the CdS-rich subcells, as previously discussed. Thus, the cells were not current-matched at this stage. However, since the above-band gap photon fluxes were similar for both cells (potential photocurrent of roughly 6 mA/cm^2), it is anticipated that the J_{sc} within a given wire was similar in both cases. For the purposes of determining V_{oc} and FF, it is this microscopic J_{sc} within a given wire that is relevant, not the J_{sc} averaged over a large area containing both contacted and uncontacted wires. Furthermore, V_{oc} and FF vary relatively slowly with J_{sc}, so small mismatches due to imprecision in the location of subcell cleaving should have a relatively small effect. Thus, the V_{oc}'s and FF's of the CdS-rich and CdSe-rich cells can be directly compared, and their V_{oc}–FF products can give a general indication of their relative performance on the single-NW level.

As shown in parentheses in Table 1, the V_{oc} and FF of every CdS-rich cell was found to exceed those of the corresponding CdSe-rich cell under filtered illumination, as expected for the wider band gap cell. Thus, the V_{oc}–FF products of the wide band gap CdS-rich cells are larger than those of the narrower band gap CdSe-rich cells. This implies that if all NWs can be contacted and the location of subcell isolation fine-tuned for optimal current-matching, the larger band gap CdS-rich cell is expected to have greater power output than the CdSe-rich cell, which is the key benefit of spectrum-splitting that enables a system of two cells to achieve higher efficiencies than the narrow gap cell on its own.

These results constitute the first proof-of-concept demonstration of a MILAMB solar cell using spatially composition-graded alloy NWs. In the future, this approach to cell fabrication for spectrum-splitting PV could provide a low cost alternative to traditional multijunction tandem cells.

Conclusion. Spatially composition-graded CdSSe NW ensemble solar cells with two subcells were fabricated in a single process flow on a single substrate. *I*–*V* testing was conducted both under AM1.5G illumination and using optical filters to simulate spectrum-splitting. The NW cells demonstrated V_{oc}'s of up to 307 and 173 mV for the CdS- and CdSe-rich cells, respectively, while the values for comparable film cells were less than 100 mV for both subcells. This is attributed to the superior optical quality of the NWs, as evidenced by micro-PL scans along the lengths of the CdSSe NW ensembles and films, showing that the ratio of band edge to defect emission was roughly 20 times higher for the NWs than in the films. The J_{sc}'s of the NW ensemble cells were quite promising for unaligned wires and approached or exceeded the thin film cells for some CdSe-rich subcells, though typical J_{sc} values for the CdS-rich NW cells were still in the range of ∼3–15 times lower than the film cells. This is attributed to SOG covering some of the wires and could be improved through strategies to obtain vertically oriented wires (such as using growth templates) or thinner SOG layers. Nonetheless, the superior optical quality of the NW materials and higher V_{oc}'s of the resulting cells indicate the ability of NWs to ultimately achieve higher efficiencies than comparable thin film cells.

I–*V* measurements were also taken using optical filters to simulate a simple form of spectrum-splitting. The wider-band gap CdS-rich subcells achieved higher V_{oc}'s and FFs than the corresponding CdSe-rich subcells for all samples under filtered illumination with both cells receiving similar above-band gap photon flux. This suggests that if all NWs can be contacted to achieve current-matching, the wider band gap subcell should produce more power than the narrower band gap subcell, which is the key benefit of spectrum-splitting that enables multiple cells to achieve higher efficiencies than a single junction.

As a first proof-of-concept study using CdSSe, no attempt was made to optimize the performance of the solar cells. Thus, our cell performance was lower than state-of-the-art nanowire-based devices. Rather, the intention of this study was to demonstrate the feasibility of fabricating MILAMB solar cells so as to lay the groundwork for future research to further improve the device design, optimization and fabrication. Our approach and results represent a proof-of-principle demonstration of MILAMB solar cell fabrication using spatially composition-graded NWs grown in one step on a single substrate by the Dual-Gradient Method. The combination of potentially high efficiencies due to the high crystal quality of NW materials and their low cost synthesis using a single, inexpensive CVD step on

dx.doi.org/10.1021/nl502662h | *Nano Lett.* 2014, 14, 5772–5779

one substrate could make MILAMB cells an attractive approach to spectrum-splitting PV. Moreover, their potential to partially decouple the fabrication cost and complexity from the number of subcells could facilitate the addition of more junctions for achieving higher efficiencies. This could make spectrum-splitting PV systems based on MILAMB solar cells an attractive low cost alternative to traditional high-efficiency multijunction tandem cells.

Experimental Section. *Materials.* CdS and CdSe are II–VI semiconductors with direct band gaps of 2.42 and 1.74 eV, respectively.[32] Like many II–VI materials, they exhibit a strong natural preference for one doping type, in this case n-type, and are resistant to doping of the opposite type.[33] Thus, for PV applications, cells based on these materials can be more readily realized using a heterojunction with another p-type semiconductor rather than a homojunction. ZnTe was selected for this application in the present work. ZnTe is a p-type II–VI semiconductor material with a relatively wide band gap of 2.26 eV,[32] which is important for coupling light into the cell, and can be readily doped up to high effective acceptor concentrations. It has been used as the p-layer in CdSe solar cells by a number of researchers using a variety of approaches to synthesis and doping[34−36] and is judged to be the most appropriate option for the CdSSe cells in this work.

Fabrication. The fabrication process for CdSSe NW ensemble solar cells is illustrated in Figure 11, below. First,

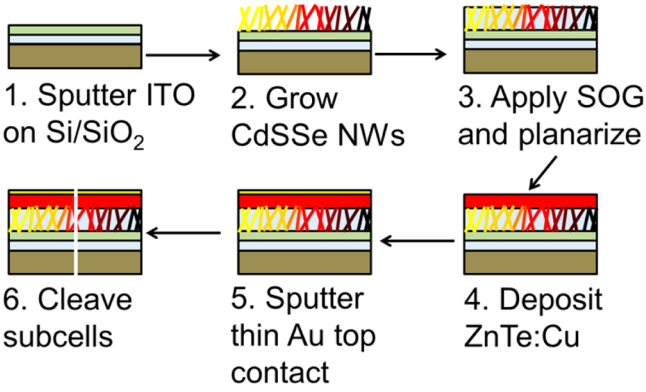

Figure 11. Fabrication process for proof-of-concept spatially composition-graded CdSSe NW ensemble solar cells.

400 nm of SiO_2 is deposited by plasma-enhanced chemical vapor deposition onto a Si(100) substrate. A layer of indium tin oxide (ITO) approximately 200 nm thick is deposited on top by radio frequency sputtering. It serves as a convenient back contact due to its compatibility with the substrate temperatures during the CdSSe growth process, which are in the range of 500–550 °C. Next, spatially composition-graded CdSSe NWs are grown by Dual-Gradient CVD using Au catalyst, as has been described in detail in previous publications.[25,26]

MSQ SOG is applied to the NW ensemble after growth by spin-coating up to a maximum spin speed of 4000 rpm. This fills the voids between wires and prevents shorting between the p-layer and back contact. The thickness of this layer is approximately 4 μm according to profilometry and cross-sectional SEM, as shown in Figure 8. The sample is baked on a hot plate at 130 °C for several minutes and then gradually ramped up to a maximum temperature of 250 °C at a rate of 200 °C/hour. This process allows the SOG to flow during the long, gradual temperature ramp for better gap-filling and cross-links the material to form a permanent insulating layer between the wires. The NWs protruding from the MSQ are planarized using a soft, textured material, and the sample is sonicated in ethanol for several minutes to prepare the substrate for subsequent depositions.

Next, approximately 100–300 nm of ZnTe and 1–2 nm of Cu are deposited by thermal evaporation in a vacuum bell jar system at 220 °C. This forms the p-type side of a p–n heterojunction with the CdSSe NWs to separate the photogenerated charge carriers in the device. Cu acts as an acceptor in ZnTe, and 220 °C was found to be the optimum temperature for dopant activation (see Supporting Information for more details). Finally, a thin layer of Au roughly 11 nm thick is sputtered on top as a semitransparent top contact (approximately 40% transparent for wavelengths in the 500–800 nm range). Note that thin metal is a convenient top contact structure at the proof-of-concept stage due to ease of fabrication but would be replaced with a more transparent contacting scheme in a practical system.

At the end of the process, the sample is cleaved at the location where the band gap of the spatially composition-graded CdSSe absorber reaches the desired value, as measured by micro-PL scan, to isolate the CdS-rich and CdSe-rich regions of the sample and form two distinct subcells in the simplest way possible in this proof of concept study. In a mature manufacturing process in the future, subcell isolation would likely be achieved through laser ablation, prepatterning of the metal catalyst, or another high-throughput, high-yield process rather than cleaving. This would leave the substrate intact and produce multiple cells monolithically on a single substrate. The location of subcell isolation would also be optimized experimentally in an iterative process of design, fabrication, and characterization to account for the real experimental performance of all electrical and optical components of the system.

The CdSSe thin film cells fabricated for comparison are synthesized in a similar process to that shown in Figure 11 for NWs, though with a few notable differences. The growth of spatially composition-graded CdSSe thin films is similar to the growth of NWs, but no Au catalyst is used. The nominal CdS and CdSe source temperatures for film growth were 900 and 780 °C, respectively, achieved by positioning the respective source boats at different positions in the reactor, while substrate temperatures were in a similar range as for NW growth. Furthermore, the application of SOG to isolate the back contact and the subsequent planarization step are not required in the case of a continuous film, so this process is forgone in the fabrication of thin film cells. All other steps shown in Figure 11 are identical.

Photoluminescence. Micro-PL measurements were conducted using a 405 nm continuous-wave laser as the excitation source, focused to a spot size of less than 50 μm. Samples were scanned at intervals of 0.5–2 mm along the lengths of the samples (the composition grading direction). All measurements were taken at room temperature.

Time-correlated single photon counting (TCSPC) measurements were also taken on pure CdSe NWs and films to measure the carrier lifetimes (see Supporting Information). TCSPC is a time-dependent PL technique for detection of low-level, short-lifetime, high-repetition rate signals. The PL emission excited by a laser of high-repetition rate is low enough such that no more than one photon in one laser signal period is detected. The arrival time of the photon in the signal period is measured.

dx.doi.org/10.1021/nl502662h | Nano Lett. 2014, 14, 5772–5779

By counting the number of the photons at different arrival times, the time distribution of the emission probability is reconstructed, which allows the lifetime to be extracted. The TCSPC measurements in this work were conducted at room temperature using a PicoQuant 405 nm laser (pulse width, 30 ps; repetition rate, 20 MHz) as the excitation source. The signal was collected using a Hamamatsu photomultiplier tube sensitive to wavelengths of 200−900 nm. The minimum detectable PL lifetime of the TCSPC instrument (Becker & Hickl) is 0.1 ns.

Current−Voltage (I−V) Characterization. The cells were mounted on glass stages, and Au wires were bonded using Ag epoxy to make electrical connection to a pair of Au electrodes for $I-V$ characterization. $I-V$ data was collected at room temperature using a temperature-controlled stage and Keithley 2420 source meter with 1 sun AM1.5G illumination provided by an Oriel class A solar simulator. A circular aperture 4 mm in diameter was placed over the cells to define an active illuminated area with which to calculate their current densities. Measurements were taken with and without optical filters, which were used to create a simple form of spectrum splitting. The optical filters were selected to transmit wavelengths shorter and longer than 620 nm for the CdS- and CdSe-rich subcells, respectively. The transmission spectra of the filters are shown in the Supporting Information.

■ ASSOCIATED CONTENT

Supporting Information

Diagram of Dual-Gradient growth process; ZnTe doping and annealing experiments; semitransparent Au top contact transmission characterization; transmission spectra of optical filters; and fabrication of pure-CdSe thin film solar cells. This material is available free of charge via the Internet at http://pubs.acs.org.

■ AUTHOR INFORMATION

Corresponding Author

*E-mail: cning@asu.edu.

Notes

The authors declare no competing financial interest.

■ ACKNOWLEDGMENTS

This material is based upon work supported in part by the National Science Foundation (NSF) and the Department of Energy (DOE) under NSF CA No. EEC-1041895. Any opinions, findings and conclusions, or recommendations expressed in this material are those of the authors and do not necessarily reflect those of NSF or DOE. We gratefully acknowledge the use of facilities within the Center for Solid State Electronics Research (CSSER) and the Leroy-Eyring Center for Solid State Science (LE-CSSS). D. Caselli gratefully acknowledges financial support from the ARCS Foundation and the Science Foundation of Arizona. Special thanks to T. Karcher for his assistance and advice with film deposition experiments; to Y. Zhang for providing access to a solar simulator and to J. Becker for assistance in its use; to P. Nichols and S. Turkdogan for their expertise with the CdSSe growth; and to all members of ASU Nanophotonics Group and research support staff at Arizona State University for all their help and support.

■ REFERENCES

(1) Moon, R. L.; James, L. W.; Vander Plas, H. A.; Yep, T. O.; Antypas, G. A.; Chai, Y. *Proceedings of the 13th IEEE Photovoltaic Specialists Conference*, Washington D.C., June 5−8, 1978; Institute of Electrical and Electronics Engineers (IEEE): Piscataway, NJ, pp 859−867.

(2) Bloss, W. H.; Griesinger, M.; Reinhardt, E. R. *Appl. Opt.* **1982**, *21*, 3739−3742.

(3) Ludman, J. E.; Riccobono, J.; Semenova, I. V.; Reinhand, N. O.; Tai, W.; Li, X.; Syphers, G.; Rallis, E.; Sliker, G.; Martin, J. *Sol. Energy* **1997**, *60*, 1−9.

(4) Imenes, A. G.; Mills, D. R. *Sol. Energy Mater. Sol. Cells* **2004**, *84*, 19−69.

(5) Russo, J. M.; Vorndran, S. D.; Zhang, D.; Gordon, M.; Wu, Y.; Kostuk, R. K. *Proceedings of the Renewable Energy and the Environment Congress*, Tucson, AZ, November 3−7, 2013.

(6) Russo, J. M.; Zhang, D.; Gordon, M.; Vorndran, S.; Wu, Y.; Kostuk, R. K. *Opt. Express* **2014**, *22*, A528−A541.

(7) Gu, T.; Haney, M. W. *Proceedings of the Renewable Energy and the Environment Congress*, Eindhoven, Netherlands, November 11−14, 2012.

(8) Atwater, H. A.; Escarra, M. D.; Eisler, C. N.; Kosten, E. D.; Warmann, E. C. *Proceedings of the IEEE Photovoltaic Specialists Conference*, Tampa, FL, June 16−21, 2013.

(9) Barnett, A.; Kirkpatrick, D.; Honsberg, C.; Moore, D.; Wanlass, M.; Emery, K.; Schwartz, R.; Carlson, D.; Bowden, S.; Aiken, D.; et al.. *Proceedings of the 22nd European Photovoltaic Solar Energy Conference*, Milan, Italy, September 3, 2007.

(10) Barnett, A.; Kirkpatrich, D.; Honsberg, C.; Moore, D.; Wanlass, M.; Emery, K.; Schwartz, R.; Carlson, D.; Bowden, S.; Aiken, D.; et al. *Prog. Photovoltaics* **2009**, *17*, 75−82.

(11) Green, M. A.; Ho-Baillie, A. *Prog. Photovoltaics* **2010**, *18*, 42−47.

(12) Xiong, K.; Lu, S.; Dong, J.; Zhou, T.; Jiang, D.; Wang, R.; Yang, H. *Sol. Energy* **2010**, *84*, 1975−1978.

(13) Wang, X.; Waite, N.; Murcia, P.; Emery, K.; Steiner, M.; Kiamilev, F.; Goossen, K.; Honsberg, C.; Barnett, A. *Prog. Photovoltaics* **2012**, *20*, 149−165.

(14) Mitchell, B.; Peharz, G.; Siefer, G.; Peters, M.; Gandy, T.; Goldschmidt, J. C.; Benick, J.; Glunz, S. W.; Bett, A. W.; Dimroth, F. *Prog. Photovoltaics* **2011**, *19*, 61−72.

(15) Wallentin, J.; Anttu, N.; Asoli, D.; Huffman, M.; Åberg, I.; Magnusson, M. H.; Siefer, G.; Fuss-Kailuweit, P.; Dimroth, F.; Witzigmann, B.; et al. *Science* **2013**, *339*, 1057−1060.

(16) Sun, K.; Kargar, A.; Park, N.; Madsen, K. N.; Naughton, P. W.; Bright, T.; Jing, Y.; Wang, D. *IEEE J. Sel. Top. Quantum Electron.* **2011**, *17*, 1033−1049.

(17) Cui, Y.; Wang, J.; Plissard, S. R.; Cavalli, A.; Vu, T. T. T.; van Veldhoven, R. P. J.; Gao, L.; Trainor, M.; Verheijen, M. A.; Haverkort, J. E. M.; et al. *Nano Lett.* **2013**, *13*, 4113−4117.

(18) Garnett, E.; Yang, P. *Nano Lett.* **2010**, *10*, 1082−1087.

(19) Garnett, E.; Brongersma, M.; Cui, Y.; McGehee, M. *Annu. Rev. Mater. Res.* **2011**, *41*, 269−295.

(20) Kapadia, R.; Fan, Z.; Takei, K.; Javey, A. *Nano Energy* **2012**, *1*, 132−144.

(21) Kempa, T. J.; Day, R. W.; Kim, S. K.; Park, H. G.; Lieber, C. M. *Energy Environ. Sci.* **2013**, *6*, 719−733.

(22) Kelzenberg, M. D.; Turner-Evans, D. B.; Putnam, M. C.; Boettcher, S. W.; Briggs, R. M.; Baek, J. Y.; Lewis, N. S.; Atwater, H. A. *Energy Environ. Sci.* **2011**, *4*, 866−871.

(23) Shin, J. C.; Lee, A.; Mohseni, P. K.; Kim, D. Y.; Yu, L.; Kim, J. H.; Kim, H. J.; Choi, W. J.; Wasserman, D.; Choi, K. J.; et al. *ACS Nano* **2013**, *7*, 5463−5471.

(24) Mohseni, P. K.; Behnam, A.; Wood, J. D.; Zhao, X.; Yu, K. J.; Wang, N. C.; Rockett, A.; Rogers, J. A.; Lyding, J. W.; Pop, E. *Adv. Mater.* **2014**, DOI: 10.1002/adma.201305909.

(25) Pan, A. L.; Liu, R. B.; Sun, M.; Ning, C. Z. *ACS Nano* **2010**, *4*, 671−680.

(26) Pan, A. L.; Zhou, W.; Leong, E. S. P.; Liu, R. B.; Chin, A. H.; Zuo, B.; Ning, C. Z. *Nano Lett.* **2009**, *9*, 784−788.

(27) Caselli, D. A.; Ning, C. Z. *Opt. Express* **2011**, *19*, A686−694.
(28) Ning, C. Z.; Pan, A. L.; Liu, R. B. *Proceedings of the 34th IEEE Photovoltaic Specialists Conference*, Philadelphia, PA, June 7−12, 2009; Institute of Electrical and Electronics Engineers (IEEE): Piscataway, NJ, pp 001492−001495.
(29) Kuykendall, T.; Ulrich, P.; Aloni, S.; Yang, P. *Nat. Mater.* **2007**, *6*, 951−956.
(30) Nichols, P. L. Ph.D. Dissertation, Arizona State University, December 2012.
(31) Wang, K.; Rai, S. C.; Marmon, J.; Chen, J.; Yao, K.; Wozny, S.; Cao, B.; Yan, Y.; Zhang, Y.; Zhou, W. *Nanoscale* **2014**, *6*, 3679−3685.
(32) Berger, L. I. In *CRC Handbook of Chemistry and Physics*, 93rd ed.; Haynes, W.M., Ed.; CRC Press/Taylor and Francis: Boca Raton, FL, 2013; pp 12-80−12-93.
(33) Desnica, U. V. *Prog. Cryst. Growth Charact.* **1998**, *36*, 291−357.
(34) Buch, F.; Fahrenbruch, A. L.; Bube, R. H. *Appl. Phys. Lett.* **1976**, *28*, 593−595.
(35) Patel, N. G.; Panchal, C. J.; Makhija, K. K.; Patel, P. G.; Patel, S. S. *Cryst. Res. Technol.* **1994**, *29*, 247−252.
(36) Pal, A. K.; Mondal, A.; Chaudhuri, S. *Vacuum* **1990**, *41*, 1460−1462.